

Nurul Khakhim¹, Agung Kurniawan², Widodo Setiyo Pranowo³

Morphodynamic Cartography Visualization of Wulan River Estuary Systems from Space to Numerical Approach Based on Multi-Season Analysis


Abstract: This research aims to investigate the morphodynamics of the Wulan River estuary in Demak Regency using the integration of multispectral remote sensing images and numerical modeling. In this study, PlanetScope for a manual-visual analysis of estuary morphodynamics and Sentinel-2 MSI Level 2A to obtain periodic total suspended solids (TSS) information for the east and west monsoon seasons. MIKE by DHI software used to develop hydrodynamic numerical modeling in order to characterize the current circulation and sediment transport model. Based on a marine cartography aspect, the obtained results illustrated that the climatological phenomenon of seasonal forcing plays a role in the development of the current circulation and indirectly influences the sediment transport. During the west season, the morphodynamics in the Wulan River estuary are much more massive and significant as compared to the east season. A projection of the deposition that results from the sediment transport is described in the bed-thickness change; this occurs in the western part of the Wulan River estuary during the east season, while the bed-thickness change occurs predominantly in the northern part during the west season (where there was previously a beach sandbar phenomenon). This was verified through multi-temporal satellite imagery that the deposition that occurs in the northern part of the Wulan River estuary during the west season is increasingly progressive and massive.

Keywords: estuary, Wulan River, morphodynamics, remote-sensing imagery, numerical modeling, marine cartography


Received: November 6, 2023; accepted: September 20, 2024

2024 Author(s). This is an open-access publication, which can be used, distributed, and reproduced in any medium according to the Creative Commons CC-BY 4.0 License

¹ Universitas Gadjah Mada, Faculty of Geography, Department of Geographical Information Science, Yogyakarta, Indonesia, email: nurulk@ugm.ac.id (corresponding author),

 <https://orcid.org/0009-0001-4046-8690>

² Universitas Gadjah Mada, Faculty of Geography, Postgraduate Geography, Coastal and Watershed Management Planning, Yogyakarta, Indonesia, email: agung.kurniawan.16@mail.ugm.ac.id,

 <https://orcid.org/0000-0002-2441-8706>

³ National Research and Innovation agency (BRIN), Research Center for Climate and Atmosphere, Bandung, Indonesia, email: widodo.pranowo@gmail.com,  <http://orcid.org/0000-0002-5798-4181>

1. Introduction

Estuaries and coasts are natural systems that are useful for civilization, making them one of the most threatened ecosystems globally [1, 2]. They act as ecological links between land and marine ecosystems and are influenced by the hydrodynamics of estuaries, including the phenomena of tides, currents [3, 4], and periodic circulations from upstream through river systems (which results in lower salinity levels) [5]. Sometimes, bio-geomorphic phenomena also play active roles in building these ecosystems [6]. Morphological changes in estuaries are closely related to sediment transport phenomena [7], where the sedimentation that occurs in estuaries is generally due to erosion phenomena in higher upstream systems; the resulting material is carried by river flows toward the estuaries and interact directly with coastal currents and waves [8]. The main driving force for sediment transport phenomena and other materials in estuarine waters is influenced by longitudinal and vertical circulations [9, 10].

An actual identification of changes in coastal morphology due to sedimentation transport phenomena can be done using remote-sensing time-series data [11–13]. Meanwhile, another approach that has been proposed and is commonly used is numerical modeling for estimating sediment transport by fluids due to the circulation of the water masses that arise due to the forces that are caused by tides, waves, wind, and salinity [7]. In sediment-transport models, understanding this cannot be based on individual events, as morphological changes along a coast obscure their contribution to the general evolution of the coastline (and coastal thrusts vary widely) [14].

Zhang et al. [10] stated that changes in morphology in an estuary cause changes in the general circulation of the estuary. Apart from this, they also affect the lateral circulation and the feedback on the longitudinal circulation of the estuary by changing the lateral advection. Through the studies that were conducted by [14], a numerical model was built to represent the mechanism of cross-shore sediment transport that is caused by waves and storms; this model consisted of sub-models of wave transformations, morphodynamic movements, and sedimentation to represent transport by considering the grain-size redistribution. On the other hand, Colina Alonso et al. [15] explained the sediment-transportation process that builds a tidal system that is formed by a mixture of sand and mud (where these two materials will experience erosion and transportation simultaneously). As a result, sand-mud interactions result in morphological changes to tidal basins (with a major influence on erosion) so that these interactions increase the formation of mud flats.

In general, studies on evolution in estuaries have mostly been carried out using numerical-modeling approaches [7, 16, 17]. Another approach that is also possible to use is spacecraft-based; namely, using remote-sensing data. Yuan et al. [18] investigated the morphodynamic variability of the Lin-gang tidal flat (Shanghai) using remote-sensing images from various sources in a multi-temporal manner by extracting water lines. The results of the investigations that were carried out show the existence of sequential accretion and erosion phenomena. The distribution of total suspended

solids (TSS) is also a study that is related to the morphodynamic phenomena on coasts; such research was carried out by Febrianto and Latifah [19] and Jiyah et al. [20], who utilized visible channel multispectral imagery to compute the TSS distribution in waters. However, a combination of both approaches is also visible in several recent studies – especially the identification of the TSS distribution in waters combined with the numerical modeling of current circulation around estuaries and coasts [21, 22]. In this study, the results of investigations based on multispectral remote sensing images to obtain TSS values were then combined with coupled models in numerical modeling to identify the evolution of the water topography in the estuaries and the surrounding ecosystem (which is still being affected by estuary tidal phenomena).

This study was applied to one of the estuaries on the north coast of Java – specifically, the Wulan River estuary (or Wulan Delta). The massive sedimentation in this estuary results in the addition of wetlands around the intertidal zone [23]. Monitoring and projections of sediment loads are needed in order to control future ecosystem problems in the Wulan River estuary [24]. Through the study of [25], sedimentary material from the mainland is influenced by tidal energy, which is then distributed by longshore currents right in front of the estuary mouth in a lateral zig-zag pattern. In general, the dominance of bottom sediments in the waters of the Wulan Delta is fine silt with an asymmetrical shape and being well-sorted, which then settles due to the low wave energy processes [26]. Previous research was generally carried out while considering only one particular time and did not consider seasonal variations. Seasons definitively influence the precipitation regime, which can increase the sediment material on land and its flow into estuaries [27]. A better understanding of the hydrodynamic phenomena and sedimentation in the Wulan River needs to be simulated by considering the influence of seasonal variations; this was carried out comprehensively in this study and supported by remote-sensing data resources and visualized based on a marine cartography approach.

2. Methodology.

Remotely-sensed Data Source and Sediment Concentration Transformation Formula

Remote-sensing data plays a role in digital-based transformation and manual analysis to describe the evolution of estuary morphology in general. This study used two types of imagery with different resolutions: PlanetScope imagery was used for manual-visual analysis (with a spatial resolution of 3 m), and a digital analysis was carried out using Sentinel-2 satellite imagery (with a spatial resolution of 10 m). The difference in the data sources was because PlanetScope was a relatively new satellite image with a more detailed resolution than Sentinel-2 offered, so it was suitable for manual-visual interpretation. Unfortunately, PlanetScope imagery is not yet available on cloud-computing platforms such as Google Earth Engine (GEE). In this study, the entire digital TSS computation was carried out on the cloud using GEE,

so the Sentinel-2 image was chosen. The manual-visual interpretation was carried out by utilizing interpretation keys to separate water and land objects as well as the land that arose as a result of the sediment-deposition process. A combination of RGB channels was used to make it easier to find the interpretation key, as it could display actual colors. The PlanetScope imagery was obtained under the academic and research scheme of PlanetLabs (<https://www.planet.com/>). In conducting a sediment-concentration analysis in the waters based on Sentinel-2 satellite imagery, this study used a combination of equations that were developed by Laili et al. [28] as an original equation. It was modified using the suggestions from Zhao et al. [29], with ratio bands that involved Rrs_{green} and Rrs_{red} being added to the equation. We obtained the TSS values on the satellite images by using Equation (1):

$$\text{TSS [mg/L]} = 31.42 \frac{Rrs_{\text{green}}}{Rrs_{\text{red}}} - 12.719 \quad (1)$$

The image that was used was Harmonized Sentinel-2 MSI (MultiSpectral Instrument, Level-2A), which is a product that has undergone atmospheric correction to the surface-reflectance (SR) level and was geometrically corrected referring to the 1984 UTM/WGS projection (<https://sentinels.copernicus.eu/web/sentinel/user-guides/sentinel-2-msi/product-types/level-2a>). The entire series of computing processes was carried out on the GEE platform, where the program code was built using the JavaScript programming language [30]. By using a cloud-computing platform such as GEE, one can emphasize efficiency in storage use and computing time [31]. This study involved a large data constellation where Sentinel-2 image data was taken at the peak of the west season (January) and the peak of the east season (July) (or, the image with the least cloud disturbance, and the recording time that was closest to both seasons each year from 2017 to 2023).

3. Site Study and Numerical Model Setup

The study area in this research specifically targeted the Wulan River Estuary pilot project, which is on the western coast of Demak Regency (Fig. 1). The Wulan River is a tributary of the Lusi and Serang Rivers where these two river flows join and are accommodated by the Klambu Dam, which is located in Grobogan Regency, Central Java. Then, the Wulan River flows toward the Wilalung sluice gate, which has nine individual sluice gates. This sluice gate was originally built during the Dutch colonial period and is located in Babalan Hamlet, Kalirejo Village, Undaan District, Kudus Regency, Central Java [32]. The estuary of the Wulan River is astronomically located at $6^{\circ} 44' 04''$ S and $110^{\circ} 32' 14''$ E. The study area is still included in the shallow water category, where the maximum depth reaches 46 m below sea level. The waters of the Wulan River estuary will directly contact the water masses of the Java Sea and Semarang Bay. The total area of this research area is 187.81 km²; the length

of the coastline in the domain area is 38.14 km, while it is 20.24 km long in the northern domain, 12.82 km long in the western domain, and 12.39 km long in the southern domain. Through an analysis of tidal conditions, the waters around the Wulan River estuary can be identified as a diurnal tide (Fig. 2) with a FormZahl number value of 3.51. The tidal data was predicted using the global tide model for the height data (with a resolution of 0.125×0.125 degrees).

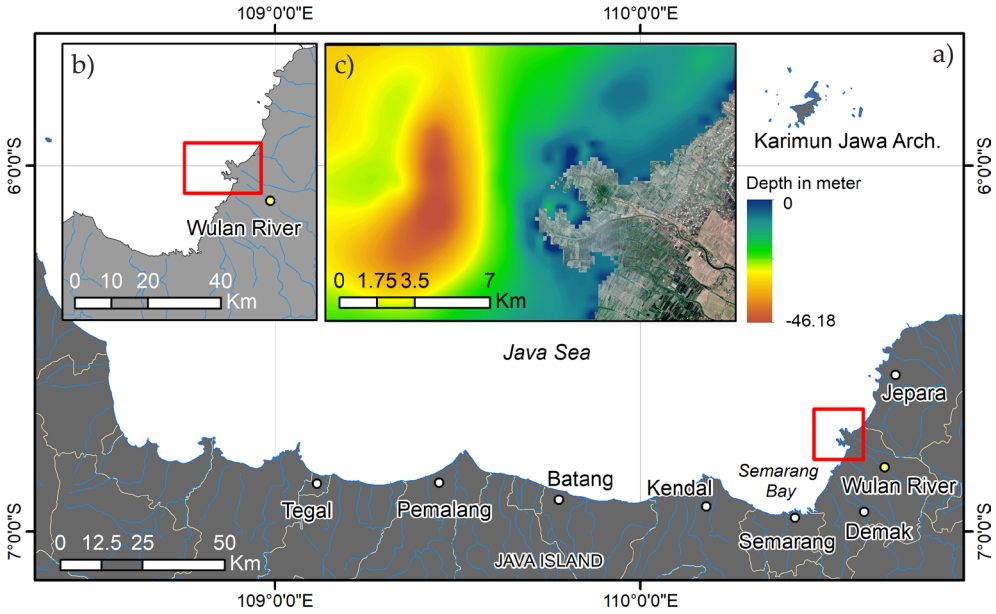


Fig. 1. Study area: island of Java with Demak district marked with a red box (a) and more detailed subset into Demak Regency (b); bathymetry information from BATNAS [35] (c)

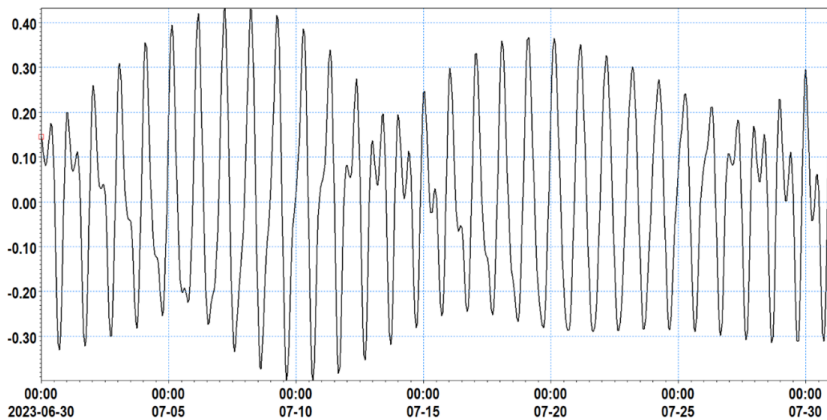


Fig. 2. Tidal graph in Wulan River estuary area

A local tidal analysis shows that the Demak waters fall into the micro-tidal category (within a tidal range of up to 1.3 m). In this study, the tidal data along the domain was used as a hydrodynamic generator, which was added to wind data that was simulated simultaneously in the development of a barotropic-based hydrodynamic model. Apart from the hydrodynamics (HD) module, spectral waves (SW) and sand-transport (ST) were simulated simultaneously in this study (also known as a coupled-model). The modeling system is based on the numerical solution of the two/three-dimensional incompressible Navier–Stokes equations, taking Boussinesq assumptions and hydrostatic pressure into account using MIKE software (by DHI).

The continuity equation that was used in this research was as follows:

$$\frac{\partial u}{\partial x} + \frac{\partial v}{\partial y} + \frac{\partial w}{\partial z} = S \quad (2)$$

along with the following two horizontal momentum equations for the x and y components, respectively:

$$\begin{aligned} & \frac{\partial u}{\partial t} + \frac{\partial u^2}{\partial x} + \frac{\partial uv}{\partial y} + \frac{\partial wu}{\partial z} = \\ & = fv - g \frac{\partial \eta}{\partial x} - \frac{1}{\rho_0} \frac{\partial p_a}{\partial x} - \frac{g}{\rho_0} \int_z^n \frac{\partial \rho}{\partial x} dz - \frac{1}{\rho_0 h} \left(\frac{\partial s_{xx}}{\partial x} + \frac{\partial s_{xy}}{\partial y} \right) + F_u + \frac{\partial}{\partial z} \left(V_t \frac{\partial u}{\partial z} \right) + u_s S \end{aligned} \quad (3)$$

$$\begin{aligned} & \frac{\partial v}{\partial t} + \frac{\partial v^2}{\partial y} + \frac{\partial uv}{\partial x} + \frac{\partial wv}{\partial z} = \\ & = -fv - g \frac{\partial \eta}{\partial y} - \frac{1}{\rho_0} \frac{\partial p_a}{\partial y} - \frac{g}{\rho_0} \int_z^n \frac{\partial \rho}{\partial y} dz - \frac{1}{\rho_0 h} \left(\frac{\partial s_{yx}}{\partial x} + \frac{\partial s_{yy}}{\partial y} \right) + F_v + \frac{\partial}{\partial z} \left(V_t \frac{\partial v}{\partial z} \right) + v_s S \end{aligned} \quad (4)$$

where:

- t – time,
- x, y, z – Cartesian coordinates,
- u, v, w – flow velocity components,
- h – depth,
- f – Coriolis parameter,
- F_u, F_v – horizontal stress terms based on gradient-stress relation,
- $u_s S, v_s S$ – effect of mass sources or sinks on the u and v components,
- S – magnitude of the discharge due to point sources,
- g – gravitational acceleration,
- ρ – density of water,
- ρ_0 – reference density of water.

In general, this model will be simulated continuously for the 2022 east (June through August 2022) and west (December 2022 through February 2023) seasons. The simulation will be run on an unstructured mesh (Fig. 3) with the specific information is given by Table 1. The input wind data as external forcing that was used in the model domain was obtained via ECMWF ERA5 (<https://cds.climate.copernicus.eu/datasets>), which is a point series. The position of the virtual wind station is still around the model domain at the following coordinates: 6° 47' 24" S and 110° 27' 0" E (Fig. 4b).

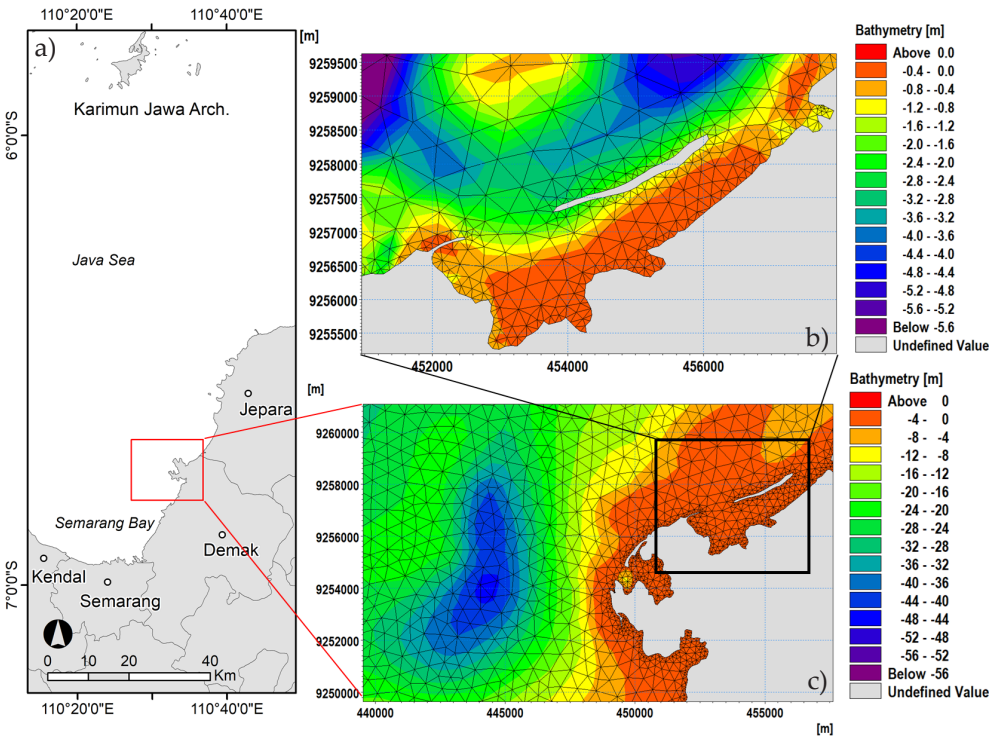


Fig. 3. Wulan River location (a), unstructured mesh used in modeling where detailed aspects of coastline are taken into consideration (b), and including results of existing sedimentation deposits that form sandbanks (c)

Table 1. Specifications of unstructured mesh in modeling domain

Description	Number
Number of elements	4,970
Smallest allowable angle	27
Total number of nodes	2,826

The number of elements describes the total number of triangles, the smallest allowable angle aims to control the skewness of the triangles, and the total number of nodes is the whole node for constructing the unstructured mesh. The model in this study was run for two seasons (east and west) so that the wind-input data adjusted the time series of the seasonal periods. During the east season, it can be seen that the prevailing wind moves from the southeast to the northwest, while it can be seen that the prevailing wind flows from the northwest to the southeast during the west season (Fig. 4).

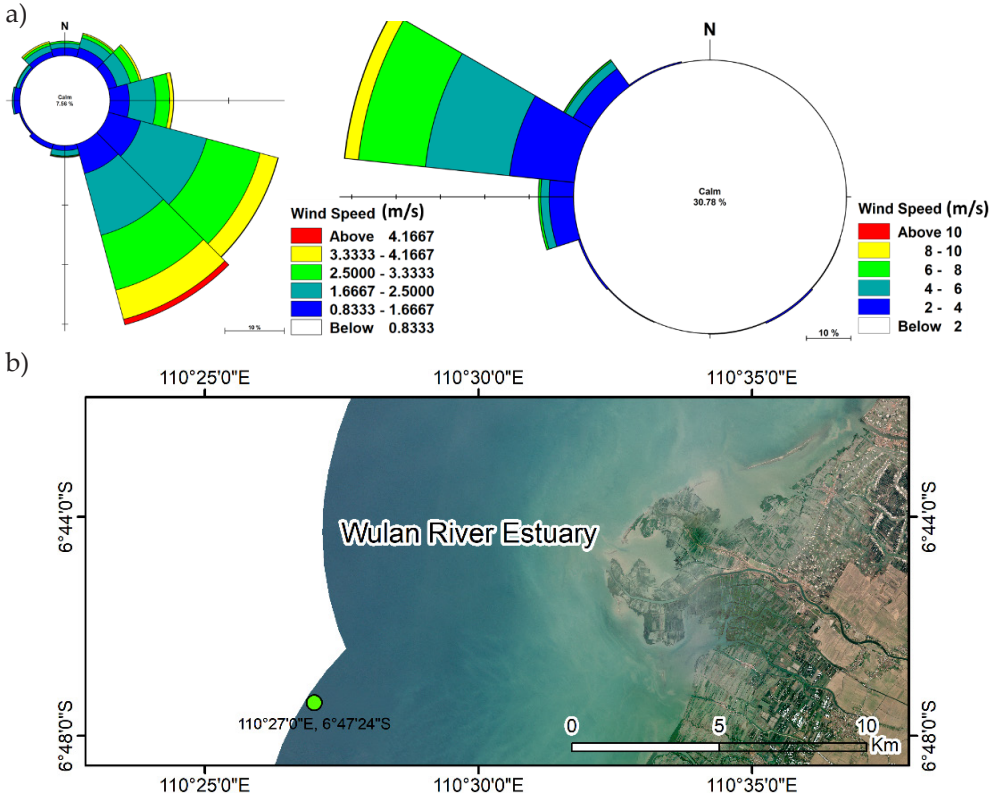


Fig. 4. Windrose during east season (left) and west season (right) (a); position of virtual wind station (green point) (b)

The wind speed during the west season was identified as being much stronger than the wind during the east season; the maximum speed during the west season was >10 m/s, while it was >4 m/s during the east season. Winds and tides were the main input in building the current circulation model for the hydrodynamics (HD) module in this study with barotropic-based density, where the density is projected as a function of salinity and temperature (which was considered to be constant during the modeling) [33]. The eddy viscosity was run with the Smagorinsky formula [34],

which was constant at 0.28. A constant value was chosen because the bathymetry around the study area tends to be gentle and there are no sudden changes in the bathymetry. This model defined topographic layers in the form of a constant Manning number. The wind input that was used based on the season was prepared in a time-varying format.

Apart from the HD module, waves were defined using the SW module to explain the wave transformation in the Wulan River estuary. The formulation that was used was quasi-stationary formulation. The surface water elevation and current were directly connected to the previous HD module. The bottom friction in this study was Nikuradse roughness (k_N), which was constant at 0.04 m. In describing the estuary morphodynamics, the mud transport (MT) module was added. The selection of this module was based on the high level of turbidity around the estuary. The sediment transport in the MT module came from advection-diffusion calculations in the HD module. The MT module solved the advection-diffusion equation, which is formulated as follows [36]:

$$\frac{\partial \bar{c}}{\partial t} + u \frac{\partial \bar{c}}{\partial x} + v \frac{\partial \bar{c}}{\partial y} = \frac{1}{h} \frac{\partial}{\partial x} \left(h D_x \frac{\partial \bar{c}}{\partial x} \right) + \frac{1}{h} \frac{\partial}{\partial y} \left(h D_y \frac{\partial \bar{c}}{\partial y} \right) + Q_L C_L \frac{1}{h} - S \quad (5)$$

where:

- \bar{c} – depth averaged concentration [g/m^3],
- u, v – depth averaged flow velocities [m/s],
- D_x, D_y – dispersion coefficients [m^2/s],
- h – depth [m],
- S – deposition/erosion term [$\text{g}/\text{m}^3/\text{s}$],
- Q_L – source discharge per unit horizontal area [$\text{m}^3/\text{s}/\text{m}^2$],
- C_L – concentration of the source discharge [g/m^3].

In the MT module, this study used two parameters for fractions and layers. The settling parameters used flocculation, while the deposition parameters used the Teeter profile. Erosion was defined as “soft mud,” with the driving waves being obtained from the SW module simulation.

4. Results and Discussion

4.1. Remote-sensing Approach Analysis

A manual-visual interpretation analysis was carried out using a combination of visible channels (namely, RGB) on the PlanetScope images. This study analyzed at least 14 image packages that were obtained from the Global Monthly Basemap Series that was provided by PlanetScope. The evolution of the Wulan River estuary ecosystem is clearly visible, with the appearance of coastal sandbars in the north.

With the manual-visual interpretation analysis involving interpretation keys, the evolution of the estuary was characterized by the appearance of sediment deposition around the estuary. The interaction of physical motion in the estuary with the deposition process will be discussed further in the discussion section. Figure 5 shows a constellation of the PlanetScope image data at the peaks of the west season (namely, during each January from 2017 through 2023). In this series of images, it can be seen that the evolution of the Wulan River estuary ecosystem occurs predominantly in the north during the west season; this is indicated by the occurrence of fluctuations in the accumulation of sedimentary material and the formation of a temporary inter-tidal land.

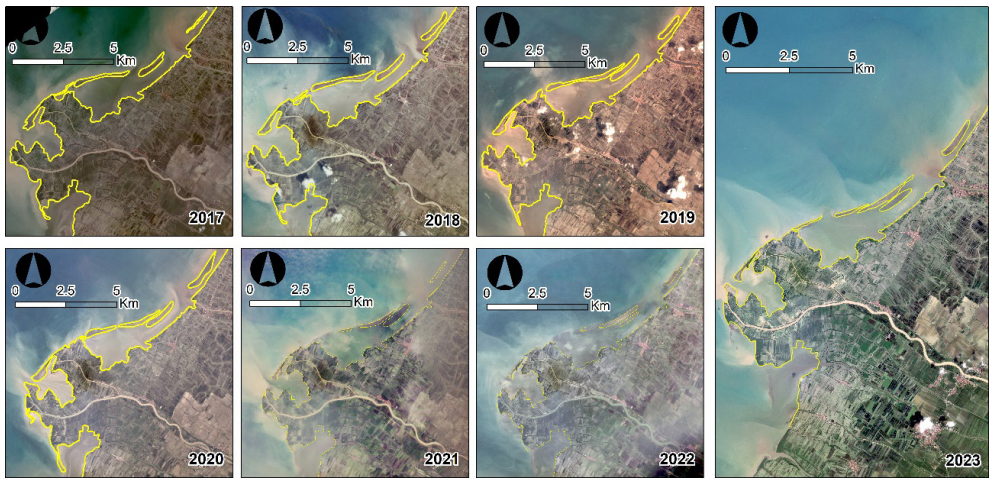


Fig. 5. Morphological evolution in Wulan River estuary during west seasons from 2017 through 2023; yellow line represents water's boundary with land

Apart from the buildup of sedimentary material in the northern part of the Wulan River estuary, there was a phenomenon that is strongly suspected to be an erosion event where part of the land area was massively eroded; namely, in the southern part of the Wulan River estuary (Fig. 6).

Another identification was also carried out at the peak of the east season, with image representation taken from each July from 2017 through 2023. Based on a manual-visual interpretation analysis, it can be identified that the deposition that occurred during the east season in the area north of the Wulan River estuary did not occur. This is significant when compared to the previous western season (Fig. 7).

During the east season, the erosion phenomenon in the southern part of the Wulan River estuary still appeared like that which was found during the west season (and in the same relative location). Figure 8 shows the erosion phenomenon that occurred in the southern part of the Wulan River estuary.

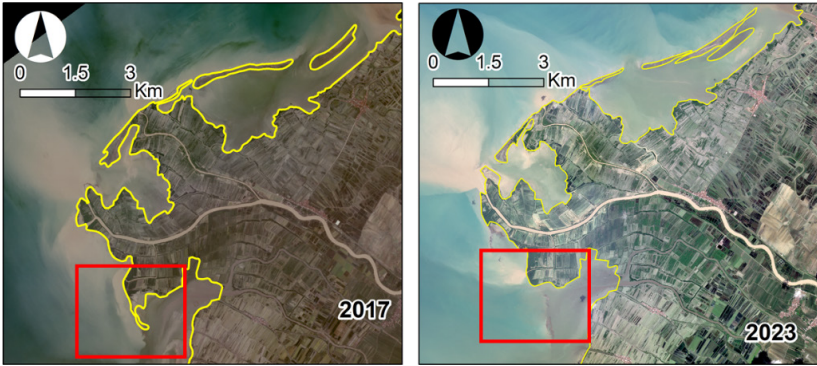


Fig. 6. Identification of erosion phenomena around Wulan River estuary during west season

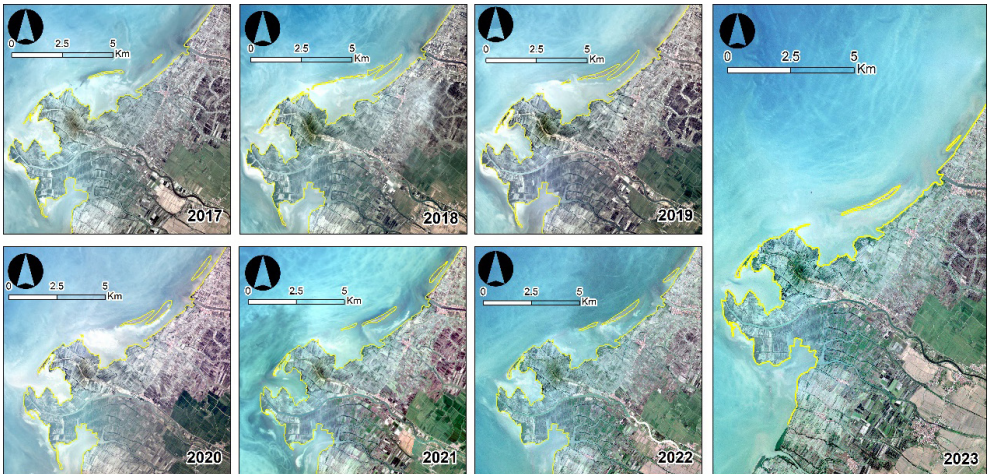


Fig. 7. Morphological evolution in Wulan River estuary during east seasons from 2017 through 2023; yellow line represents water's boundary with land

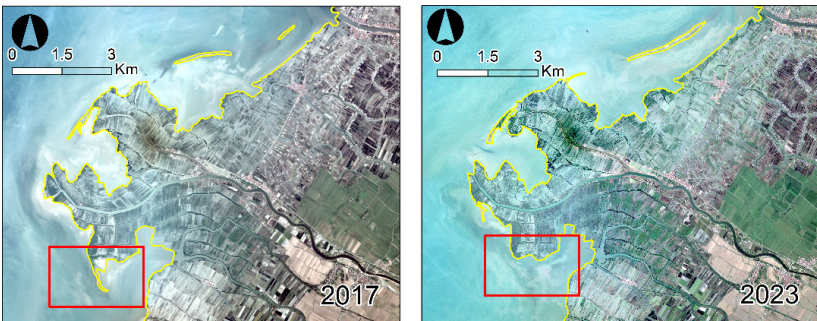


Fig. 8. Identification of erosion phenomena around Wulan River estuary during east season

Digitally, an approach that used a formula that was developed by [28, 29] was used to identify the total suspended solids (TSS) in the waters of the Wulan River estuary. The image that was used in the digital-based analysis to identify the sediment concentrations was Sentinel-2 (which was corrected to the surface-reflectance level). The entire series of digital processing and transformation processes was carried out via the cloud platform (Google Earth Engine – GEE). To separate the land objects from the water, we used the NDWI digital-transformation approach in GEE. Figure 9 shows the TSS results that were extracted from the Sentinel-2 image data from the 2022 east season and 2023 west season.

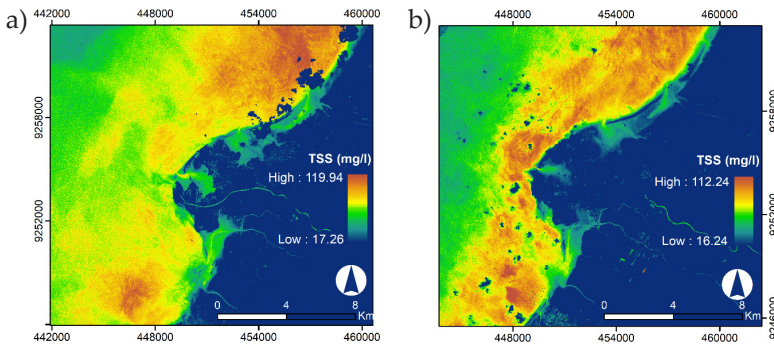


Fig. 9. TSS calculation results based on Sentinel-2 satellite imagery during east season in 2022 (a) and west season in 2023 (b)

The striking difference in the TSS that were extracted from the two seasons was the distributions of the TSS concentrations in the waters around the Wulan River estuary. During the eastern season, high TSS concentrations could be found in the north and south of the Wulan River estuary; during the west season, however, high TSS concentrations could be found along the coast that surrounded the Wulan River estuary ecosystem. The highest TSS value that was identified during the east season was 119.9 mg/L, and the lowest was 13.76 mg/L. During the west season, the highest TSS concentration was slightly lower (namely, 112.2 mg/L), and the lowest was 16.2 mg/L. The results from this TSS calculation were then integrated with a numerical model for further analysis. The TSS values that were obtained through the extraction method using the digital approach and the combination formula that was developed by [28, 29] tended to have lower results when compared with the studies that were conducted by [20].

4.2. Numerical Model Result and Analysis During Eastern Season

The hydrodynamic model produced two main outputs: namely, surface elevation as a representation of sea level height, and current circulation in a 2D barotropic context for both seasons. During the east season (Fig. 10), the modeling results showed that, during the highest high-tide conditions, the current moved from the

northeast to the southwest, with a maximum speed that reached >0.358 m/s. Meanwhile, the current that circulated around the Wulan River estuary was relatively slow (within a range of $0.000\text{--}0.085$ m/s). The current circulation regime around the waters of the Wulan River estuary during the highest high tide was homogeneous with the overall current that came from the northeast and moved toward the southwest (giving rise to what is called a “longshore” current). Meanwhile, the current regime was divided into several patterns under the lowest ebb conditions: namely, those currents that moved at speeds of $0.0580\text{--}0.318$ m/s from the west then turned sharply to the north, and those currents with similar speeds that moved from the south toward the north. A low number of other current regimes were those that came from the northeast toward the southwest but were deflected to the west at speeds of $0.000\text{--}0.025$ m/s. Under the lowest low-tide conditions, there were indications of an eddy current in the northern part of the waters of the Wulan River estuary. Through the SW module, it can be seen that the significant wave height around the Wulan River estuary during the east season during the modeling period periodically dipped below 1 cm, where the peak significant wave height was at 0.082 m (8.2 cm) (Fig. 11).

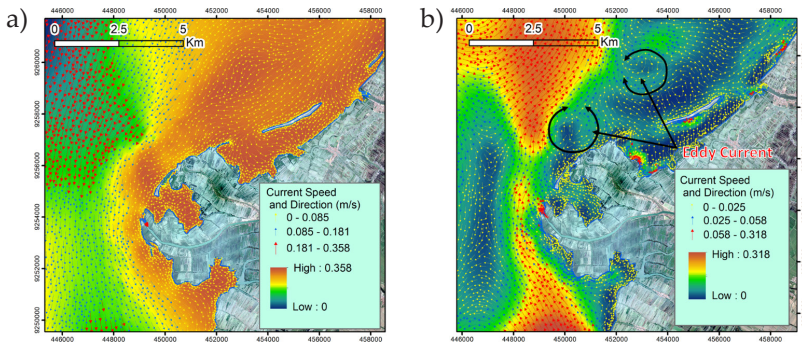


Fig. 10. Current circulation during east season at highest high tide (a) and lowest low tide (b)

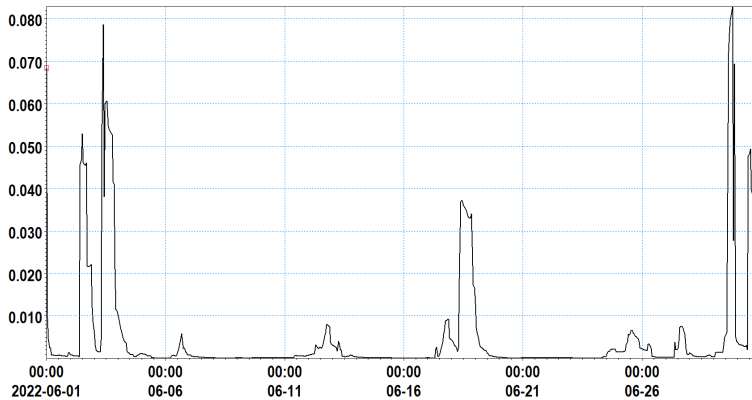


Fig. 11. Significant wave height during east season [m]

Furthermore, the data that was extracted from TSS regarding the east season was then integrated into a numerical model. We chose six points around the Wulan River estuary as TSS sources that transmitted sediment concentrations based on the TSS values that were obtained via the digital transformation of the Sentinel-2 satellite image. During the east and west seasons, the selected locations were the same; however, the TSS input value was adjusted to the season-extraction results in the image. The TSS-concentration information can be seen in Table 2 and Figure 12.

Table 2. TSS-concentration value as input to MT module

Source location (in UTM 49M)		TSS during west season [mg/L]	TSS during east season [mg/L]
449815.8659	9250271.3545	65.4	70.5
448957.4137	9251763.4179	70.6	64.1
448544.8236	9255059.9666	74.3	70.3
450484.7569	9257601.0060	76.6	77.5
454678.1880	9258275.6045	57.8	76.2
455449.7805	9260742.6075	76.8	94.8

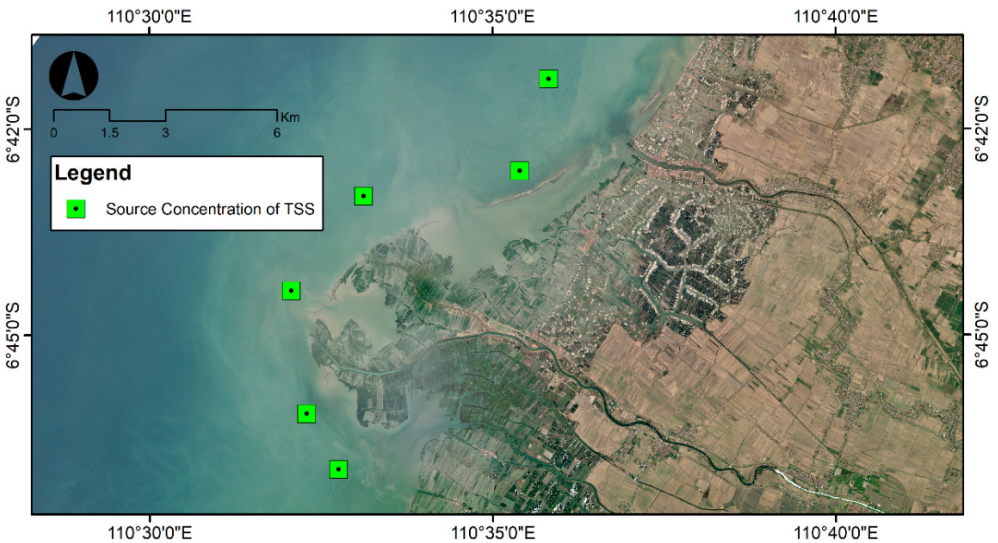


Fig. 12. Geographical plot of TSS-concentration source

The sediment transport around the Wulan River estuary during the east season can be seen through the results of the model that was run in the MT module; at the end of the modeling, it can be seen that the total suspended sediment concentration (in milligrams per litre) moved following the current circulation in the waters of the

river estuary. During the month where there were two main current regimes that moved the TSSs in the waters (namely, the currents that moved from the northeast confronted the currents that moved from the south, thus causing an eddy current. As a result, the dominant TSS materials moved in the area and eventually settled. Any material that experiences deposition then has the potential to cause changes in the thickness of the water bed (Fig. 13b). Visually, it can be seen that the material deposition had a pattern that reflected the same direction as the current circulation and was strengthened by the influence of the eddy currents on the material-deposition phenomenon (Fig. 13b – dashed square).

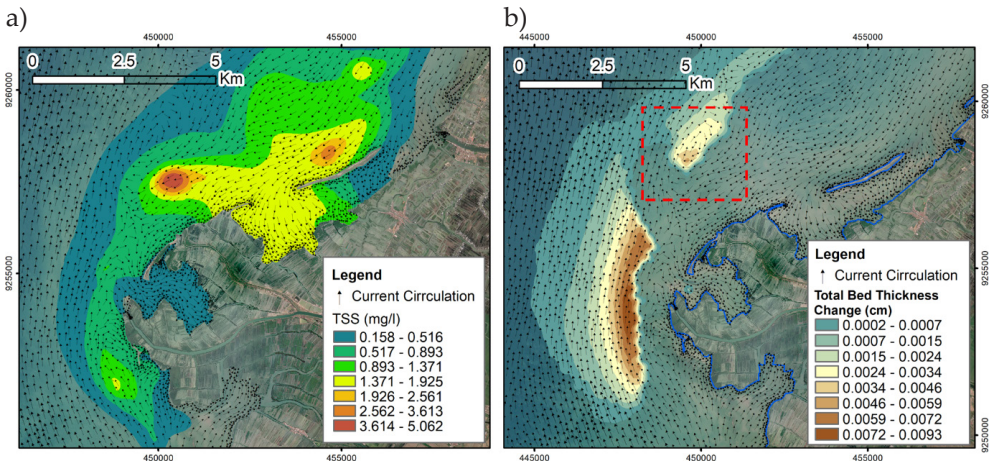


Fig. 13. TSS movement patterns followed current circulation patterns (a), and total bed thickness changed (b) in waters of Wulan River estuary during east season

4.3. Numerical Model Result and Analysis During West Season

The current circulation during the west season was obtained from the HD model in 2D form (Fig. 14). It can be seen that, under the highest high-tide conditions, the current pattern around the estuary had a circulation that moved from north to south along the coast (with a maximum speed that reached 0.073 m/s around the Wulan River mouth). In the current circulation under the highest high-tide conditions, it could be found that there was an eddy current in the northern part of the waters of the Wulan River estuary (where the eddy current moved south and passed through the narrow gap between the land and the beach sandbar that was formed due to the sedimentation). Under the lowest low-tide conditions, the current that moved along the coast reached a significant speed (reaching 0.464 m/s). Under the lowest low-tide conditions, eddy currents could also be found; they were located quite close to the eddy currents that were found during the east season. The dominant water mass came from the southwest and moved toward the northeast, but a small portion turned back to the south due to the force that was generated by the eddy currents.

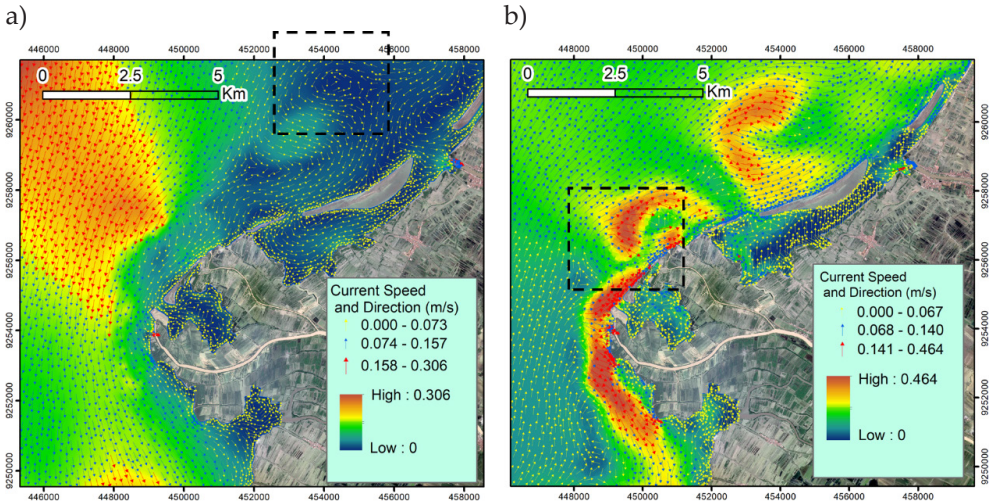


Fig. 14. Current circulation during west season at highest high tide (a) and lowest low tide (b)

During the west season, the significant wave height that was obtained from the SW module showed a varying pattern that was similar to that which occurred during the east season; during the west season, however, the peak significant wave height reached 88 cm and was much more significant when compared to the east season (Fig. 15). The wave phase also fluctuated more when compared to the previous season.

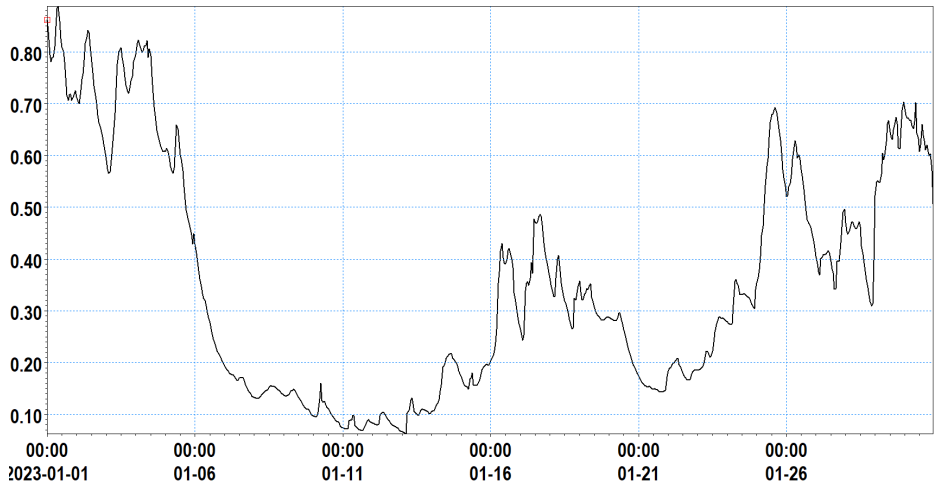


Fig. 15. Significant wave height during west season [m]

The sediment transport that was simulated in the MT module in this study showed that there was a TSS-distribution pattern that moved predominantly toward

the northeast; this was in accordance with the current circulation at that time (Fig. 16a). The suspended material that moved following the hydrodynamic patterns (Location 1) then settled and had the potential to change the thickness of the bottom layer of waters (which is referred to as a “total bed-thickness change”). Based on this analysis, the area that was projected to experience massive morphological evolution and changes was in the northern part of the Wulan River estuary or Location 2 (where there were beach sandbars that formed at this location due to the previous sedimentation processes). There were two separate beach sandbars in the northern part of the Wulan River estuary ecosystem; these sandbars were not connected due to the pushing force effect of the river discharge on the mainland. In the second coastal sandbar area, it was projected that the bottom layer of the waters would rise enough so that it was projected to merge with the land. At Location 3 (which was still part of the main ecosystem of the Wulan River estuary), it was also projected that the land area would increase because the current circulation in the area could trap and deposit sediment.

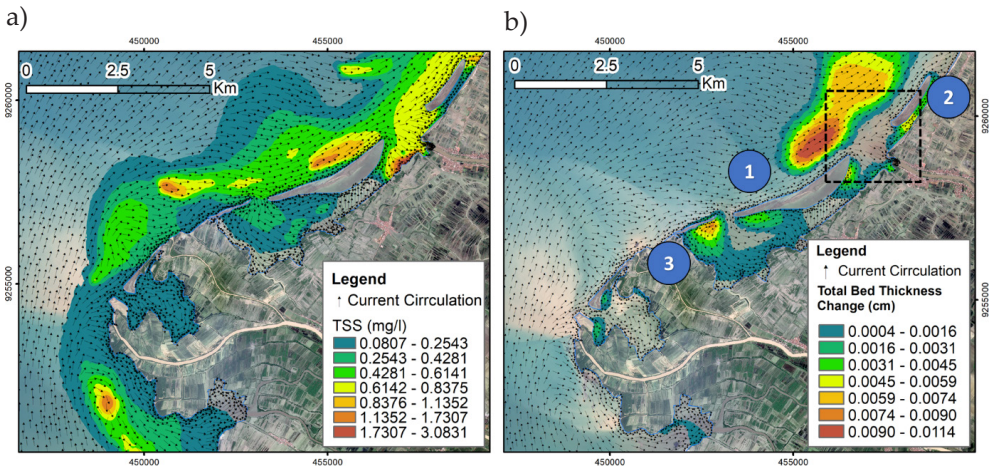


Fig. 16. TSS-movement patterns following current circulation patterns (a), and total bed-thickness changing (b) in waters of Wulan River estuary during west season; 1–3 – location points

5. Conclusion

The current circulation in the hydrodynamic process has a strong connectivity to sediment transport in a river estuary ecosystem (in this case, specifically in the Wulan River estuary). Climatological phenomena such as wind are significant driving factors in current circulation around coasts and estuaries. This could be identified through the distribution pattern of the TSS material in our study, where the currents moved from the east to the southwest during the east season due to the dominant effect of the current circulation. The projected bed thickness change was dominant in the western part of the Wulan River estuary (and vice versa during the west season).

The dominant current circulation moved from the southwest to the north so that the sediment transport would trigger deposition, thus resulting in changes in the thickness of the water bed. This phenomenon has the potential to change the morphodynamics in the northern part of the Wulan River estuary. However, it could be periodically observed that there were significant differences between the west and east seasons where, based on our observations of the remote-sensing images during the west season, the deposition that occurred in the northern part of the Wulan River estuary was much more massive than during the east season. This was also validated by the results of the sediment-transport modeling, which deposited massively in the northern part of the Wulan River estuary during the east season.

Funding

This research received no specific grant from any funding agency in the public, commercial, or not-for-profit sectors.

CRedit Author Contribution

All of the authors contributed the same amounts to each part and element of the article.

Declaration of Competing Interest

The authors declare that they have no known competing financial interests or personal relationships that could have appeared to influence the work reported in this paper.

Data Availability

Public data in this article include wind downloaded from <https://cds.climate.copernicus.eu/>, bathymetry data available at <https://tanahair.indonesia.go.id/>, and sentinel-2 MSI imagery obtained from <https://www.esa.int/>, while PlanetScope imagery data downloaded from <https://www.planet.com/> is restricted data obtained through the Education and Research Standard scheme.

Use of Generative AI and AI-assisted Technologies

No generative AI or AI-assisted technologies were employed in the preparation of this manuscript.

Acknowledgements

The authors would like to thank to DHI for providing the MIKE 21/3 software as part of a research and academic license (Student Labkit).

References

- [1] Barbier E.B., Hacker S.D., Kennedy C., Koch E.W., Stier A.C., Silliman B.R.: *The value of estuarine and coastal ecosystem services*. Ecological Monographs, vol. 81(2), 2011, pp. 169–193. <https://doi.org/10.1890/10-1510.1>.

- [2] Athanasiou P., van Dongeren A., Giardino A., Vousdoukas M.I., Ranasinghe R., Kwadijk J.: *Uncertainties in projections of sandy beach erosion due to sea level rise: An analysis at the European scale*. Scientific Reports, vol. 10(1), 2020, 11895. <https://doi.org/10.1038/s41598-020-68576-0>.
- [3] Hogueane A.M., Gammelsrød T., Mazzilli S., Antonio M.H., da Silva N.B.F.: *The hydrodynamics of the Bons Sinais Estuary: The value of simple hydrodynamic tidal models in understanding circulation in estuaries of central Mozambique*. Regional Studies in Marine Science, vol. 37, 2020, 101352. <https://doi.org/10.1016/j.rsma.2020.101352>.
- [4] Setyani F.D.: *Sediment transport study in estuary of Weriagar River, Kabupaten Teluk Bintuni, West Papua*. Jurnal Teknologia, vol. 3(1), 2020, pp. 62–71. <https://aperti.e-journal.id/teknologia/article/view/57>.
- [5] Potter I.C., Chuwen B.M., Hoeksema S.D., Elliott M.: *The concept of an estuary: A definition that incorporates systems which can become closed to the ocean and hypersaline*. Estuarine, Coastal and Shelf Science, vol. 87(3), 2010, pp. 497–500. <https://doi.org/10.1016/j.ecss.2010.01.021>.
- [6] Eulie D.O., Walsh J.P., Corbett D.R., Mulligan R.P.: *Temporal and spatial dynamics of estuarine shoreline change in the Albemarle-Pamlico estuarine system, North Carolina, USA*. Estuaries and Coasts, vol. 40(3), 2016, pp. 741–757. <https://doi.org/10.1007/s12237-016-0143-8>.
- [7] Mayerle R., Narayanan R., Etri T., Abd Wahab A.K.: *A case study of sediment transport in the Paranagua Estuary Complex in Brazil*. Ocean Engineering, vol. 106, 2015, pp. 161–174. <https://doi.org/10.1016/j.oceaneng.2015.06.025>.
- [8] Wibowo M., Hendriyono W., Rahman R.A., Susatijo G., Kongko W., Istiyanto D.C., Widagdo A.B., Nugroho S., Khoirunnisa H., Wiguna E.: *Sediment transport modeling at Jelitik Estuary, Sungailiat – Bangka Regency for the design of sediment control structures*. Journal of Physics: Conference Series, vol. 1625(1), 2020, 012042. <https://doi.org/10.1088/1742-6596/1625/1/012042>.
- [9] Kjerfve B., Stevenson L.H., Proehl J.A., Chrzanowski T.H., Kitchens W.M.: *Estimation of material fluxes in an estuarine cross section: A critical analysis of spatial measurement density and errors*. Limnology and Oceanography, vol. 26(2), 1981, pp. 325–335. <https://doi.org/10.4319/lo.1981.26.2.0325>.
- [10] Zhang R., Hong B., Zhu L., Gong W., Zhang H.: *Responses of estuarine circulation to the morphological evolution in a convergent, microtidal estuary*. Ocean Science, vol. 18(1), 2022, pp. 213–231. <https://doi.org/10.5194/os-18-213-2022>.
- [11] Temiz F., Durduran S.S.: *Monitoring coastline change using remote sensing and GIS technology: A case study of Acigöl Lake, Turkey*. IOP Conference Series: Earth and Environmental Science, vol. 44(4), 2016. <https://doi.org/10.1088/1755-1315/44/4/042033>.
- [12] Boothroyd R.J., Williams R.D., Hoey T.B., Barrett B., Prasojo O.A.: *Applications of Google Earth Engine in fluvial geomorphology for detecting river channel change*. WIREs Water, vol. 8(1), 2021, e21496. <https://doi.org/10.1002/wat2.1496>.

- [13] Zheng G., Wang Y., Zhao C., Dai W., Kattel G.R., Zhou D.: *Quantitative analysis of tidal creek evolution and vegetation variation in silting muddy flats on the Yellow Sea*. *Remote Sensing*, vol. 15(21), 2023, 5107. <https://doi.org/10.3390/rs15215107>.
- [14] Li F., Dyt C., Griffiths C.: *A coastal morphodynamic model for cross-shore sediment transport*. *WIT Transactions on the Built Environment*, vol. 70, 2003, pp. 335–344.
- [15] Colina Alonso A., van Maren D.S., van Weerdenburg R.J.A., Huisman Y., Wang Z.B.: *Morphodynamic modeling of tidal basins: The role of sand-mud interaction*. *Journal of Geophysical Research: Earth Surface*, vol. 128(9), 2023, e2023JF007391. <https://doi.org/10.1029/2023JF007391>.
- [16] Clare M.C.A., Percival J.R., Angeloudis A., Cotter C.J., Piggott M.D.: *Hydro-morphodynamics 2D modelling using a discontinuous Galerkin discretisation*. *Computers & Geosciences*, vol. 146, 2021, 104658. <https://doi.org/10.1016/j.cageo.2020.104658>.
- [17] Nguyen V.T., Vu M.T., Zhang C.: *Numerical investigation of hydrodynamics and cohesive sediment transport in Cua Lo and Cua Hoi estuaries, Vietnam*. *Journal of Marine Science and Engineering*, vol. 9(11), 2021, 1258. <https://doi.org/10.3390/jmse9111258>.
- [18] Yuan R., Zhang H., Qiu C., Wang Y., Guo X., Wang Y., Chen S.: *Mapping morphodynamic variabilities of a meso-tidal flat in Shanghai based on satellite-derived data*. *Remote Sensing*, vol. 14(16), 2022, 4123. <https://doi.org/10.3390/rs14164123>.
- [19] Febrianto S., Latifah N.: *Pemetaan pola sebaran total suspended solid (TSS) di perairan teluk Semarang Menggunakan citra satelit Landsat 7 ETM dan Landsat 8*. *Jurnal Harpodon Borneo*, vol. 10(1), 2017, pp. 56–60.
- [20] Jiyah J., Sudarsono B., Sukmono A.: *Studi distribusi total suspended solid (TSS) di perairan pantai kabupaten Demak menggunakan citra Landsat*. *Jurnal Geodesi Undip*, vol. 6(1), 2017, pp. 41–47. <https://ejournal3.undip.ac.id/index.php/geodesi/article/view/15033> [access: 12.12.2023].
- [21] Wei X., Cai S., Zhan W.: *Impact of anthropogenic activities on morphological and deposition flux changes in the Pearl River Estuary, China*. *Scientific Reports*, vol. 11(1), 2021, 16643. <https://doi.org/10.1038/s41598-021-96183-0>.
- [22] Benincasa M., Falcini F., Adduce C., Santoleri R., Sannino G.: *Remote sensing and coastal morphodynamic modelling*. [in:] *2018 IEEE International Workshop on Metrology for the Sea; Learning to Measure Sea Health Parameters (MetroSea), Bari, Italy, 8–10 Oct. 2018*, pp. 1–6, IEEE, Piscataway 2018. <https://doi.org/10.1109/MetroSea.2018.8657909>.
- [23] Ramadhani Y.H., Susanti R.: *Dynamics land cover changes of Wulan Delta in 2003–2017 approach by remote sensing technology*. *IOP Conference Series: Earth and Environmental Science*, vol. 561(1), 2020, 012042. <https://doi.org/10.1088/1755-1315/561/1/012042>.

- [24] Fadlillah L.N., Sunarto, Widyastuti M., Marfai M.A.: *The impact of human activities in the Wulan Delta Estuary, Indonesia*. IOP Conference Series: Earth and Environmental Science, vol. 148(1), 2018, 012032. <https://doi.org/10.1088/1755-1315/148/1/012032>.
- [25] Atmojo H.T., Wicaksana H.I., Rizal A., Cibaj I., Nugroho H., Ralanarko D.: *3D modelling of Longshore Bar deposit in modern fluvial dominated delta: Case study of Wulan Delta, Demak, Central Java Province*. [in:] *AAPG Datapages/ Search and Discovery, GEO-2016, 12th Middle East Geosciences Conference & Exhibition, Manama, Bahrain, March 7–10, 2016*, AAPG, Tulsa 2016, pp. 7–10.
- [26] Muskananfolo M.R., Febrianto S., Ayuningrum D.: *Hydrodynamic characteristics and sediment distribution patterns in Wulan Delta Estuary, Demak, Indonesia*. *Makara Journal Technology*, vol. 27(1), 2023, pp. 11–16. <https://doi.org/10.7454/mst.v27i1.1615>.
- [27] Wirasatriya A., Maslukah L., Indrayanti E., Yusuf M., Milenia A.P., Adam A.A., Helmi M.: *Seasonal variability of total suspended sediment off the Banjir Kanal Barat River, Semarang, Indonesia estimated from Sentinel-2 images*. *Regional Studies in Marine Science*, vol. 57, 2023, 102735. <https://doi.org/10.1016/j.rsma.2022.102735>.
- [28] Laili N., Arafah F., Jaelani L.M., Subehi L., Pamungkas A., Koenhardono E.S., Sulisetyono A.: *Development of water quality parameter retrieval algorithms for estimating total suspended solids and chlorophyll-a concentration using Landsat-8 imagery at Poteran Island water*. *The ISPRS Annals of the Photogrammetry, Remote Sensing and Spatial Information Sciences*, vol. II-2/W2, 2015, pp. 55–62. <https://doi.org/10.5194/isprsannals-II-2-W2-55-2015>.
- [29] Zhao J., Zhang F., Chen S., Wang C., Chen J., Zhou H., Xue Y.: *Remote sensing evaluation of total suspended solids dynamic with Markov model: A case study of Inland Reservoir across administrative boundary in South China*. *Sensors*, vol. 20(23), 2020, 6991. <https://doi.org/10.3390/s20236911>.
- [30] Gorelick N., Hancher M., Dixon M., Ilyushchenko S., Thau D., Moore R.: *Remote sensing of environment Google Earth Engine: Planetary-scale geospatial analysis for everyone*. *Remote Sensing of Environment*, vol. 202, 2017, pp. 18–27. <https://doi.org/10.1016/j.rse.2017.06.031>.
- [31] Amani M., Ghorbanian A., Ahmadi S.A., Kakoei M., Moghimi A., Mir-mazloumi S.M., Moghaddam S.H.A., Mahdavi S., Ghahremanloo M., Parsian S., Wu Q., Brisco B.: *Google Earth Engine cloud computing platform for remote sensing big data applications: A comprehensive review*. *IEEE Journal of Selected Topics in Applied Earth Observations and Remote Sensing*, vol. 13, 2020, pp. 5326–5350. <https://doi.org/10.1109/JSTARS.2020.3021052>.
- [32] Kanza R., Ahmada A., Darsono S., Atmodjo P.S.: *Pengendalian banjir Sungai Wulan, Demak, Jawa Tengah*. *Jurnal Karya Teknik Sipil*, vol. 6(4), 2017, pp. 300–308. <https://ejournal3.undip.ac.id/index.php/jkts/article/view/18719> [access: 12.12.2023].

-
- [33] *MIKE 21/3 Coupled Model FM: User Guide*. DHI, 2020. https://manuals.mike-poweredbydhi.help/2020/MIKE_3.htm [access: 12.12.2023].
- [34] Smagorinsky J.: *General circulation experiments with the primitive equations, I. The basic experiment*. *Monthly Weather Review*, vol. 91(3), 1963, pp. 99–164. [https://doi.org/10.1175/1520-0493\(1963\)091<0099:GCEWTP>2.3.CO;2](https://doi.org/10.1175/1520-0493(1963)091<0099:GCEWTP>2.3.CO;2).
- [35] Badan Informasi Geospasial [Geospatial Information Agency]: *Batimetri Nasional (BATNAS)*. 2024. <https://tanahair.indonesia.go.id/portal-web/login?page=/unduh/batnas> [access: 12.12.2023].
- [36] *MIKE 21 & MIKE 3 Flow Model FM, Mud Transport Module Scientific Documentation*. DHI, 2020. https://manuals.mikepoweredbydhi.help/2020/MIKE_3.htm [access: 12.12.2023].